Journal of Cluster Science (2023) 34:2977–2989
https://doi.org/10.1007/s10876-023-02434-7

ORIGINAL PAPER

One-pot Synthesis of Zeolitic Imidazole Nanoframeworks with Encapsulated *Leucas aspera* Leaf Extract: Assessment of Anticancer and Antimicrobial Activities

Prabhu Raju[1] · Manikandakrishnan Muthushanmugam[2] · Rengarajan Rengasamy Lakshminarayanan[3] · Suganthy Natarajan[4]

Received: 20 January 2023 / Accepted: 24 March 2023 / Published online: 26 April 2023

Abstract
A biocompatible nanomaterial is an essential need for medicinal applications. Zeolitic imidazole frameworks are interesting porous crystalline material which has received much attraction in the field of drug delivery due to their unique thermal/chemical stability and pH-sensitive degradability. The present study highlights the synthesis of *Leucas aspera* extract-loaded ZIF-L nanoframeworks and the assessment of its antimicrobial and anticancer efficiency. The formation of LA@ZIF-L nanoframeworks was systematically investigated by various spectroscopic and microscopic techniques. Results of the antibacterial assay exhibited antimicrobial potential against *B. subtilis, S. aureus, K. pneumonia, and P. aeruginosa* with the zone of inhibition of 18 mm, 20 mm, 17 mm, and 21 mm respectively. LA@ZIF-L showed potent anticancer potential against A549 cells with IC_{50} values of 42.61 ± 0.05 µg/mL. Cytotoxic effect of LA@ZIF-L nanoframeworks against A549 cells might be due to DNA damage induced by enhanced ROS level as observed in fluorescent microscopic studies. Brine shrimp *Artemia salina* acute toxicity assay confirmed the biocompatibility of the material. Results of *A. salina* acute toxicity assay confirmed that the LC_{50} value of nanoframeworks was observed to be 135.33 ± 2.00 µg/ml. Results conclude that ZIF-L nano framework acts as an effective drug delivery system for treatment of infection and cancer.

Keywords *Leucas aspera* (LA) · Zeolitic imidazole frameworks (ZIFs) · Antimicrobial potential · Anticancer activity · Biocompatibility

Introduction

Zeolitic imidazole frameworks (ZIFs) a subclass of metal organic framework has incessantly attracted the biomedical researchers due to its larger surface area, tunable porous structure and different topologies [1]. Unique chemical and thermal stability, high drug loading capacity, pH sensitive degradability, controlled drug release and biocompatible nature of ZIFs makes it suitable platform for drug delivery, [2-5]. Plant derived compounds-based therapeutics possess certain drawbacks such as poor solubility, non targeted drug delivery affecting the healthy tissues, short half life period, thermal instability and immune clearance. These limitations can be overcome by encapsulation of plant derived compounds or phytocompounds within ZIFs. ZIFs due to its superior stability under aqueous physiological conditions will attenuate premature degradation of phytocompound, enhance intracellular uptake and surface tailoring with targeting ligands will facilitate targeted drug delivery preventing adverse effects to healthy tissue [6]. In addition, stimuli responsive drug release, optical transparency in the visible and near IR region of ZIF makes it promising candidate for delivery of phytocompound and imaging purposes overcoming existing pharmacokinetic limitation [7-10]. This innovative strategy provides a promising solution to overcome the drawbacks in Ayurvedic therapy in which plant-based drugs are used for the treatment wide variety of human ailments

✉ Suganthy Natarajan
suganthy.n@gmail.com; suganthyn@alagappauniversity.ac.in

[1] BioMe Live Analytical Centre, Karaikudi, Tamil Nadu, India

[2] Department of Animal Health and Management, Alagappa University, Karaikudi, Tamil Nadu, India

[3] Rashtriya Uchchatar Shiksha Abhiyan (RUSA 2.0) Scheme, Madurai Kamaraj University, Madurai 625021, India

[4] Department of Nanoscience and Technology, Alagappa University, Karaikudi, Tamil Nadu, India

[11, 12]. Production of nanomaterials from plant extracts are more stable, eco-friendly and less expensive [13, 14]. *L. aspera*a a common weed ubiquitously found in India and Philippines, traditionally reported for its antipyretic, insecticide, antimicrobial, prostaglandin inhibitory and cytotoxic activities, have been taken for the present study [15-17]. Leaf extract was known to cure psoriasis, rheumatism and skin eruptions. Leaf stem extract was used for the treatment of nasal congestion, fever, cough and snake bites [18-20]. The whole plant is enriched with various phytocompounds such asursolic acid, sitosterol, diterpenes, glycosides, linifolioside, nicotine, apigenin and machilin C [21]. Previous reports in our lab highlight the encapsulation plant derived compounds such as methyl gallate, catechin and fucoidan within the ZIF-L nanoframeworks which exhibited potent anticancer, antibacterial and mosquito larvicidal activities [22-24]. Based on these facts, the present study focuses on loading *L. aspera* leaf extract within ZIF-L (LA@ZIF-L) nanoframeworks and evaluate its antimicrobial and anticancer potential.

Materials and Methods

Chemical Used

Zinc Nitrate Hexahydrate, Mueller Hinton Agar, Nutrient Broth, Penicillin, Streptomycin, DMEM High-Glucose Medium, Bovine Serum Albumin, 2-Methyl Imidazole were purchased from Himedia laboratories, India. DAPI stain and MTT were purchased from Sigma Aldrich. All chemicals and reagents used are of analytical grade. A549 human lung cancer cells were obtained from National Center for Cell Science (NCCS), Pune, India.

Preparations of *L. Aspera* Extract Powder

Green and fresh *L. aspera* (LA) leaves were collected from Alagappa University, Science campus garden. About 20 g of leaves was ground by mortar and juice was collected and freeze dried in lyophilizer. The dried extract powder was stored in air tight container under cold condition (− 20 °C) until further use.

Synthesis of *L. Aspera* Extract Loaded ZIF-L Nanoframeworks

The LA@ZIF-L nanoframeworks were prepared based on the methodology of [24], with slight modifications. Briefly, 400 mg of zinc nitrate hexahydrate and 800 mg of 2-methyl imidazole powder were dissolved separately in 50 mL of DD water and sonicated at room temperature. Fifty milliliter of 2-methyl imidazole solution was slowly added drop by drop into zinc nitrate solution and subjected to agitation for half an hour. Visual color transition to white colored colloid indicates the formation of ZIF-L nanoframeworks. About 10 mL of *L. aspera* powder solution (2 mg/mL) were slowly added into ZIF-L colloid and the agitation was continued for another 30 min. Finally, the light green colored colloidal solution was obtained. The excess number of precursors was removed by centrifugation at 8000 rpm for 30 min. The hydrated colloidal sample was dried using hot air oven at 60 °C for 6 h.

MTT Assay

Antiproliferative effect of LA@ZIF-L nanoframeworks against A549 line cells was assessed by MTT assay [22]. A549 lung cancer cells were treated with various doses of LA@ZIF-L nanoframeworks (10–100 µg/mL) for 48 h. After incubation period, cells were treated with 50 µL of MTT (0.5 mg/mL) for 4 h at 37 °C followed by treatment with 100 µL of DMSO for dissolution of blue colored formazan. The absorbance was recorded using ELISA multiplate reader (Molecular Device Spectramax M3, equipped with Softmax Pro V5 5.4.1 software) at 570 nm wavelength. Percentage of cell viability was calculated.

Assessment of ROS Generation

Intracellular reactive oxygen species generation (ROS) of LA@ZIF-L nanoframeworks treated A549 lung cancer cells were estimated by using DCFH-DA (2,7-diacetyl dichloro fluorescein acetate) fluorescent dye. Cells seeded in 96 well plate was treated with IC_{50} concentration of LA@ZIF-L nanoframeworks for 24 h at 37 °C for 30 min. After the treatment, cell containing medium was washed with Phosphate Buffer Saline solution. The fluorescence intensity of DCFH-DA in treated cells was measured by fluorescence spectrophotometer (Cary Eclipse, Varian) with emission/excitation wavelength of 480/530 nm. Cell images were taken by using fluorescent microscope (Carl Zeiss Axio Observer Z1, Germany) at 20X magnification range.

DAPI Staining Assay

Changes in nuclear morphology of LA@ZIF-L treated A549 cells were investigated by DAPI staining method [25]. Cells treated with LA@ZIF-L nanoframeworks at its IC_{50} concentration was incubated with DAPI (2 mg/mL) for 20 min. Excess amount of stain was removed by PBS wash followed by measurement of fluorescence intensity at emission/excitation wavelength of 350/460 nm. Morphological changes of treated cell images were captured in fluorescent microscopy (Carl Zeiss Axio Observer Z1, Germany) at 20X magnification.

Antibacterial Activity of LA@ZIF-L Nanoframeworks

The antibacterial potential of fabricated LA@ZIF-L nanoframeworks was systematically investigated against human pathogens such as gram-positive bacteria *Staphylococcus aureus, Bacillus subtilis* and gram-negative bacteria *Klebsiella pneumoniae*, *Pseudomonas aeruginosa* by well-cut method [25]. Overnight culture (0.1%) was evenly swabbed on the surface of Muller Hinton Agar plates and loaded with various doses of LA@ZIF-L nanoframeworks (30—120 µg/mL) and incubated overnight at 37 °C. The zone of inhibition was measured and represented in diameter.

Minimum Bactericidal Concentration

Minimum inhibitory concentration (MIC) of LA@ZIF-L and LA extract alone against *P. aeruginosa, and S. aureus* bacterial strains were determined by microdilution method in Nutrient Broth (HiMedia, India). Briefly, bacterial cultures were inoculated in nutrient broth, incubated at 37 °C for 3 h at 180 rpm. After the incubation period the culture optical density was assessed at 600 nm. 10 µL of bacterial culture of 0.4 optical density i.e. 10^6 CFU/mL were treated with various concentrations of LA@ZIF-L and LA extract alone (10 – 2560 µg/mL) and incubated overnight at 37 °C. The concentration of wells without visible growth of bacterial cells is considered as MIC, which is measured by taking optical density at 600 nm by using ELISA plate reader. Experiments were done in triplicates.

Safety Evaluation Studies

In Vitro *Safety Evaluation of LA@ZIF-L*

Antiproliferative effect of LA@ZIF-L was assessed using human peripheral blood mononuclear cells (PBMC) by MTT assay. PBMC cells were isolated from blood of healthy volunteers in accordance to methodology of Ilavarasi et al., [26]. Cells were treated with various doses of LA@ZIF-L nanocomposite (25–400 µg/mL) at 37 °C for 24 h. After incubation periods cells were subjected to PBS wash followed by MTT assay. Hydrogen peroxide (100 µM) was used as positive control.

Artemia Salina Acute Toxicity Bioassay

Bio-safety nature of synthesized LA@ZIF-L nanoframeworks was evaluated by brine shrimp *Artemia salina* lethality bioassay [27, 28]. The experimental procedure was carried out according to OECD guidelines and methods for drugs and nanomaterials [29]. Freshly hatched *A. salina* nauplii were separated as six groups of 20 Nos in 12 well plate and exposed to different concentrations of LA@ZIF-L nanoframeworks (40–200 µg/mL) in sea water for 24 h. Well containing *A. salina* naupli without LA@ZIF-L is considered as a negative control for comparative studies. The number of death and surviving organisms are counted by using magnification lens. The commercial anticancer drug cisplatin was considered as a positive control. The same concentrations (40–200 µg/mL) of cisplatin were treated against *A. salina* nauplii. The lethality rate LC_{50} of treated groups was calculated by comparison of number of survivors and deaths in treated and control groups. The percentage of lethality was calculated by using Abbott's formula:

$$\%\ \text{of lethality} = \frac{\text{Nt} - \text{Nc}}{\text{Nc}} \times 100$$

Nt and Nc—number of surviving *Artemia salina* naupli in treated group and control group.

Statistical Analysis

The IC_{50}, LD_{50} and LD_{90} values were calculated using Probit analysis software and the comparative study of biological activities between treated and control groups were done by one-way analysis of variance (ANOVA) using SPSS 17.0 software. Results were considered significant at the level of $p < 0.05$. Mean ± S.D. values was calculated from the results of triplicate experiments.

Results and Discussion

Synthesis and Characterization of the LA@ZIF-L Nanoframeworks

The formation of LA@ZIF-L nanoframeworks was confirmed by visual color transformation of reaction mixture from the white color to pale green color. In one pot synthesis method, methyl and hydroxyl groups present in the bioactive compound of *L. aspera* extract powder acted as a reducing agent facilitating the formation of ZIF-L. Formation of LA@ZIF-L nanoframeworks was further confirmed by UV–VIS spectroscopy (Fig. 1). The characteristic absorption peak of *L. aspera* extract was observed at 201 nm, while ZIF-L alone showed peak at 211 nm. LA@ZIF-L showed characteristic absorption peak at 216 nm, which indicates the change in the absorbance might be due to encapsulation of *L. aspera* extract within ZIF-L frameworks.

Characteristic functional groups of LA@ZIF-L nanoframeworks and ZIF-L frameworks were further identified by Fourier Transform Infrared (FTIR) spectroscopy (Fig. 2). FTIR spectrum of LA@ZIF-L nanoframeworks was found to be similar to the spectrum of ZIF-L nanoframeworks except

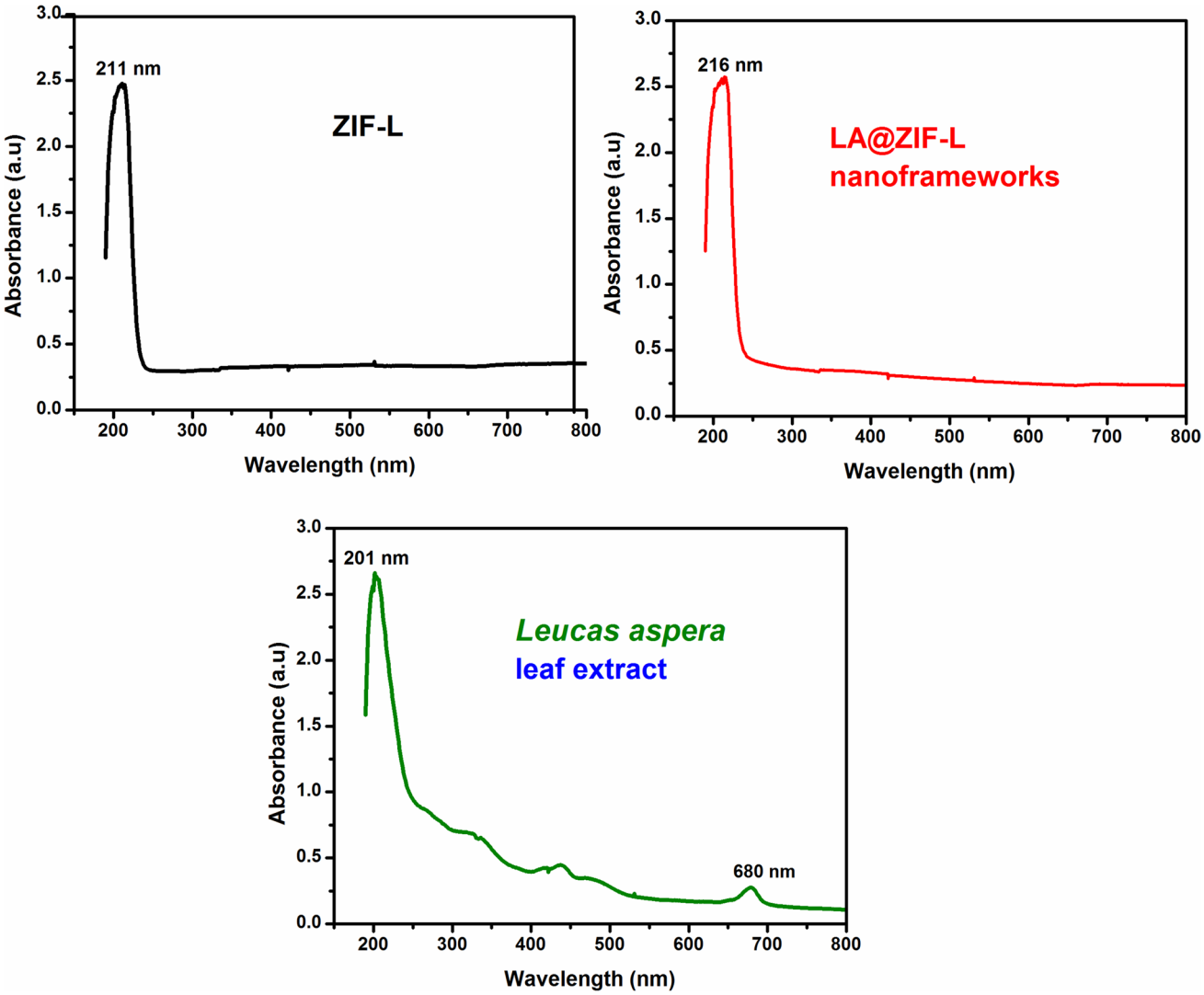

Fig. 1 UV–Vis spectrum of LA@ZIF-L (red), ZIF-L (black), LA extract (green)

some additional peaks. The sharp peaks observed at 430 and 439 cm^{-1} corresponded to the Zn–N stretching vibration of zinc ions connected with 2-methyl imidazole nitrogen group (covalent bond). The maximum absorption peaks at 704, 716, 951 and 1004 cm^{-1} corresponding to C–N stretching in imidazole linker [30]. Shift in the absorption peak from 1622 cm^{-1}, 1004 cm^{-1} to 1513 cm^{-1} in ZIF-L to 1634, 952 and 1502 cm^{-1} in LA@ZIF-L nanoframeworks might be due to presence of *L. aspera* extract inside the ZIF-L frameworks The small peaks at around 1622 cm^{-1} and 1634 cm^{-1} represents C=O stretching vibrations of amide and carboxyl groups in organic compounds such as imidazole and *L. aspera* plant extract. The peaks at 2298, 2872 cm^{-1} were assigned to C–C stretching and C–H stretching of imidazole units of ZIF-L [9, 10, 24]. Finally, the broad peaks at around 3317, and 3725 cm^{-1}attributes to the presence of hydroxyl group O–H bending vibrations.

The crystalline structure and crystalline size of the as prepared LA@ZIF-L nanoframeworks and *L. aspera* plant extract powder was investigated by using powder XRD analysis technique. PXRD patterns of LA@ZIF-L nanoframeworks showed distinct higher diffraction peaks at 14.99°, 16.95°, 21.65°, 25.73°, 27.72°, 29.07°, 30.88°, 31.48°,33.47°, 35.27°, 38.30°, 40.56°, 42.56°, 43.16 and 46.04° indexing the Bragg's reflection planes at (100), (101), (101), (110), (103), (200), (201), (004), (202), (104), (203), (114), (212), (204) and (213) according to the JCPDS number 01–1136, depicting hexagonal crystal structure (Fig. 3). Powder XRD pattern of *L. aspera* extract did not show any diffraction peaks, which indicates amorphous nature due to the presence of organic compounds in the extract. The morphology and particle size of synthesized nanoframeworks was examined by SEM and TEM microscopic techniques and the results are shown in Fig. 4. SEM and TEM images

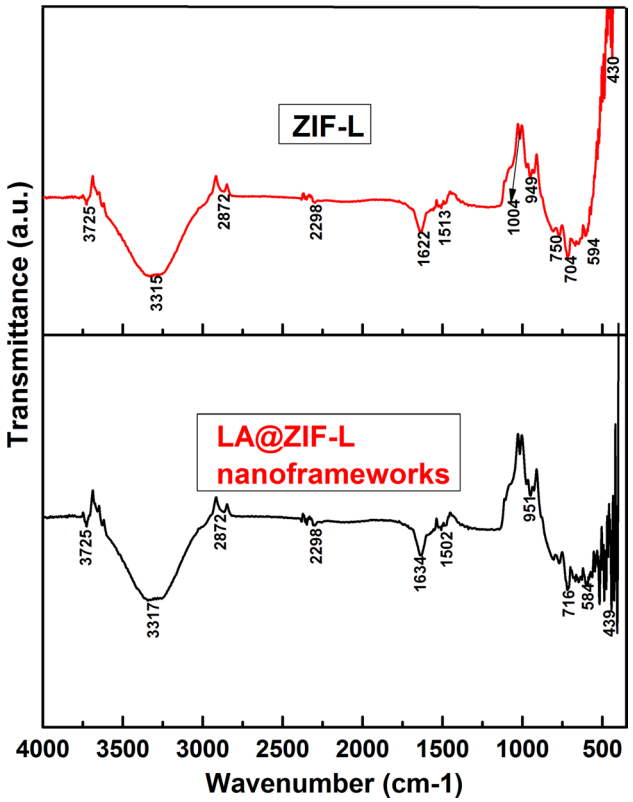

Fig. 2 FTIR spectrum of ZIF-L (red), LA@ZIF-L (black)

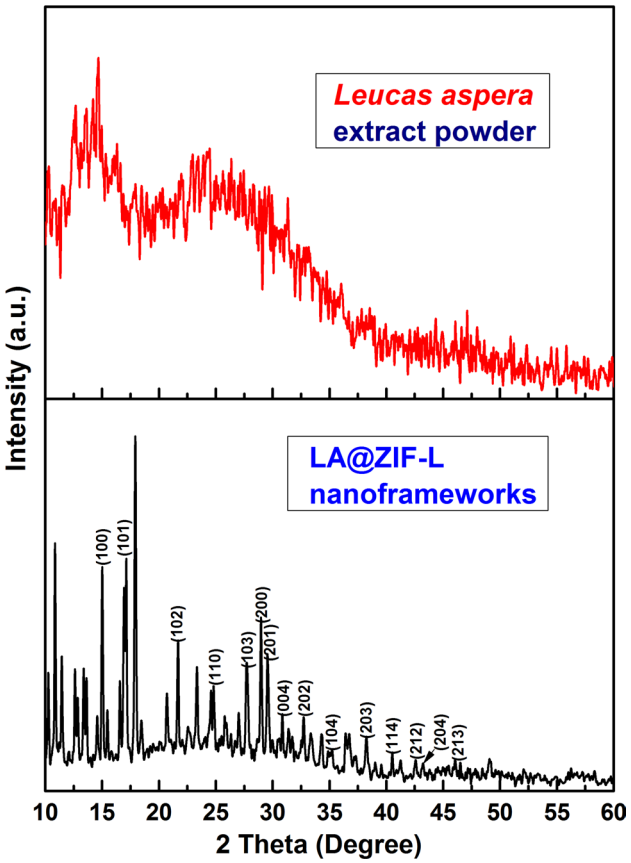

Fig. 3 Powder XRD analysis of LA@ZIF-L (black) and LA extract powder (red)

of ZIF-L alone showed distinct two-dimensional nano flaky crystal structure (Figs. 4A, C) which indicates the uniformity of crystal formation. However, microscopic images of LA@ZIF-L nanoframeworks showed agglomerated spongy particles with irregular shape (Fig. 4B, D) which might be due to disturbance in the nucleation of crystal formation caused by the incorporation of *L. aspera* extract within ZIF-L framework. The average particle size of ZIF-L and LA@ZIF-L nanoframeworks calculated from TEM analysis was observed to be 180 nm and 132 nm respectively. Reduction in the particle size of LA@ZIF-L nanoframeworks might be due to reducing properties of phytoconstituents present in the leaf extract of *L. aspera.*

Particle Size Analysis

Size of nanoparticle plays a key role in determining the cellular uptake due to its impact on enthalpic and entropic properties that influences the adhesion strength between nanoparticles and cellular receptors. In addition, size also determines the cellular uptake pathway as well as its toxic potential on living cells [31, 32]. Nanoparticles with size 200–500 nm are internalized into the cell via caveolae-mediated pathway without any sequestration with lysosomes and reticuloendothelial system [33]. In the present study the average particle size of synthesized LA@ZIF-L nanoframeworks was observed to be 250 nm (Fig. 5), which can enter into the cell via caveolae-mediated internalization mechanism as per the above reports indicating it as suitable nanoplatform for biomedical applications.

Assessment of Cytotoxic Effects of LA@ZIF-L Nanoframeworks

Cytotoxic effects of alone ZIF-L, *L. aspera* extract and LA@ZIF-L nanoframeworks against A549 lung cancer cells were investigated using by MTT assay. Treatment with LA@ZIF-L and *L. aspera* extract exhibited toxic effect in dose dependent manner, when compared to alone ZIF-L, positive control and vehicle control cells. IC_{50} values of LA@ZIF-L, *L. aspera* extract and positive control were observed to be 42.61 ± 0.05, 72.5 ± 0.07, 68.34 ± 0.05 µg/mL respectively (Fig. 6A). LA@ZIFL nanoframeworks exhibited enhanced cytotoxic effect, when compared to ZIF-L alone and positive control cisplatin, which might be due to synergistic effect of bioactive components of *L. aspera* extract. Phase contrast microscopic images revealed morphological changes in LA@ZIF-L treated groups and the results are shown in

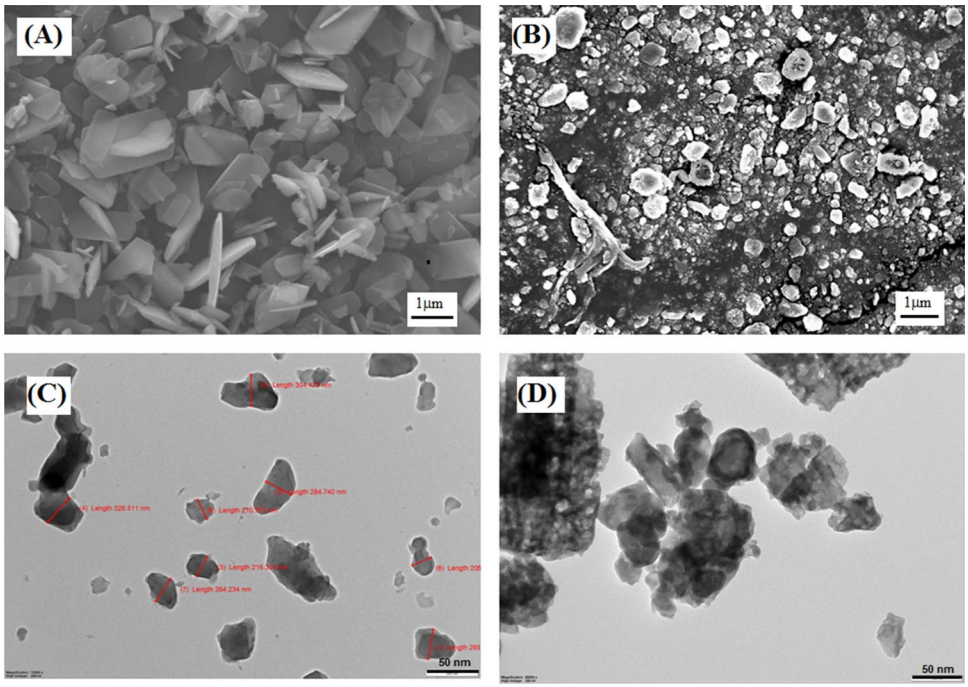

Fig. 4 **A**, **B** SEM and **C**, **D** TEM images of LA@ ZIF-L nanoframeworks

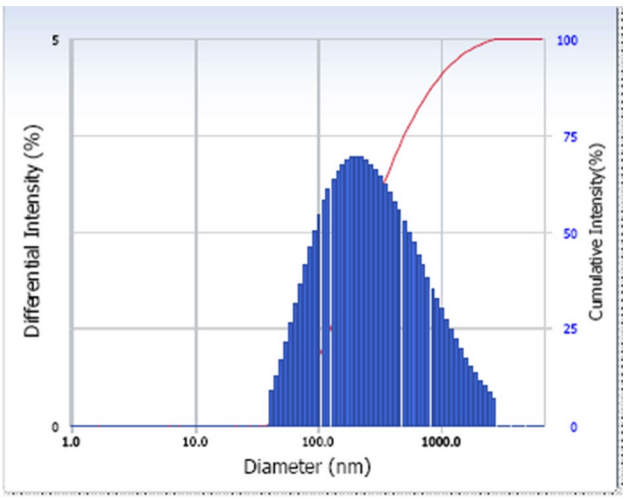

Fig. 5 DLS particle size analysis of LA@ZIF-L nanoframeworks

Fig. 6B. Reduction in cell density with rounded and shrinked cell morphology associated with membrane damage the characteristic features of apoptosis [34] was observed in LA@ZIF-L, LA extract, positive control and ZIF-L treated groups, while the control cells showed clear epithelial morphology with intact membrane and cell to cell adhesion. Overall results revealed that antiproliferative effect of LA@ ZIF-L is due to apoptosis mediated cell death.

LA@ZIF-L Nanoframeworks Induced ROS Generation in A549 Cells

Intracellular ROS acts as double-edged sword, regulating the cell signaling pathway and also inducing oxidative stress mediated cellular damage. Majority of chemotherapeutic drugs acts by tuning redox homeostasis enhancing the ROS level thereby activating apoptotic signaling pathway leading to cell death, [24, 35]. Hence the current study focuses on evaluating the intracellular ROS level in LA@ ZIF-L nanoframeworks treated groups. Fluorescent microscopic technique showed enhanced fluorescent intensities in LA@ZIF-L, positive control and *L. aspera* extract treated cells, when compared to control group and ZIF-L treated cells (Fig. 7B), which concluded that bioactive compound present in the extract enhanced the ROS levels in treated cells. Quantification of ROS production illustrated that, the fluorescent intensities of LA@ZIF-L nanoframeworks and positive control treated cells, was observed to be five-fold and 3-fold higher when compared to control cells and ZIF-L frameworks, (Fig. 7A). Results conclude that LA@ ZIF-L nanoframework induced cytotoxicity in A549 cells by enhancing the intracellular ROS level activating the apoptotic pathway.

Nuclear Damages of A549 Cells Post Exposure of LA@ZIF-L Nanoframeworks

Anticancer proficiency of chemotherapeutics is based on ROS mediated nuclear damage leading to cells death mechanisms. Recent study revealed that nanoparticles

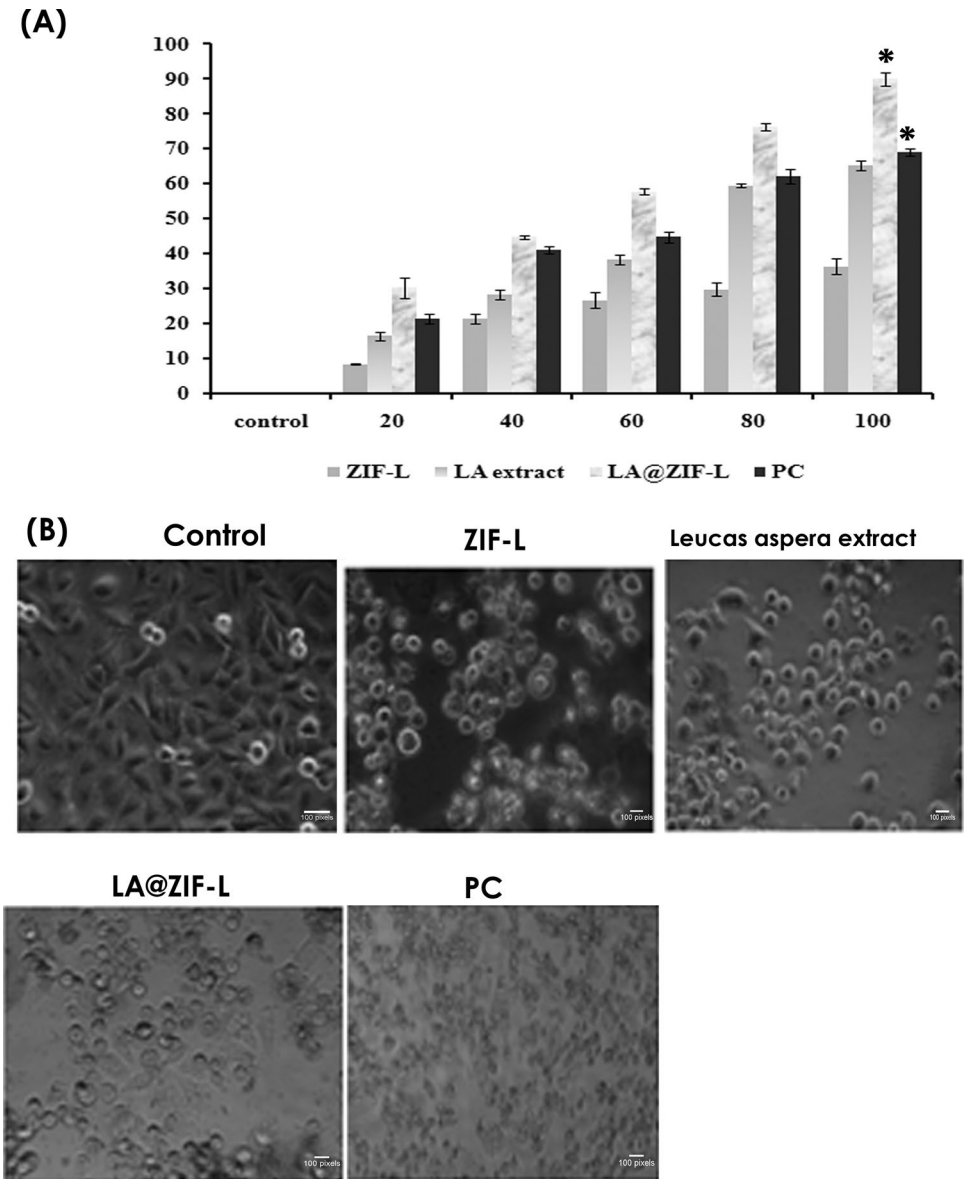

Fig. 6 **A** Assessment of cytotoxic effect of LA@ZIF-L nanoframeworks against A549 lung cancer cells by M TT assay; **B** Phase contrast microscopic images illustrating apoptotic features induced by LA@ZIF-L

exposed cell exhibited ROS burst, leading to protein oxidation, DNA fragmentation and lipid peroxidation cumulatively causing cell death [36–38]. Based on this concept, to evaluate whether apoptosis is induced by nuclear damage, DAPI staining was carried out and the results were shown in Fig. 8. Result revealed that control cells showed light blue fluorescence with intact nucleus and cytoplasm, while LA@ZIF-L nanoframeworks, positive control and *L. aspera* extract treated cells exhibited intense blue fluorescence indicating the presence of fragmented nuclei. In addition, LA@ZIF-L nanoframeworks treated cells showed many cytological changes such as nuclear shrinkage, micronuclei, binucleation and chromatin fragmentation, which confirmed that the cells were committed to death by apoptosis (Fig. 8B). The percentage of abnormal and normal nuclei in the control and treated cells are depicted in Fig. 8A. LA@ZIF-L nanoframeworks, positive control and *L. aspera* extract treated cells showed 84%, 73% and 51% abnormal nuclei when compared to negative control and ZIF-L treated cells. The results of DAPI staining indicate that LA@ZIF-L nanoframework induced ROS mediated nuclear damages in A549 lung cancer cells leading to cell death. Based on the literature survey, researchers utilized the ethanolic extract of *Leucas aspera* for anticancer applications. Some studies demonstrated that *L. aspera* extract mediated nanoparticle synthesis and its antimicrobial and anticancer applications [39, 40]. Till date there are no reports regarding encapsulation of *L. aspera* extract within

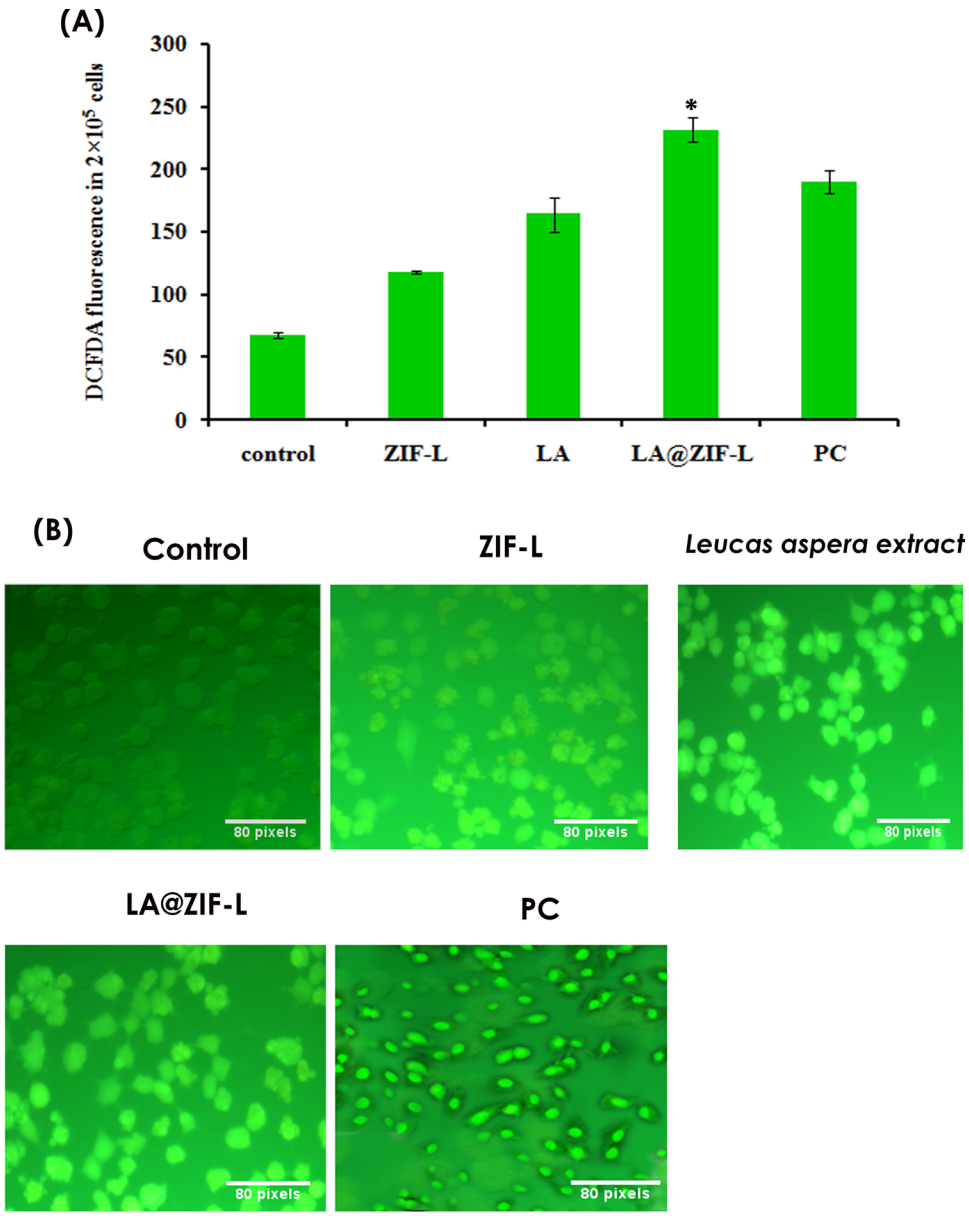

Fig. 7 **A** Quantification of ROS level in A549 cells using fluorescence spectroscopy; **B** Microscopic images of A549 cells post exposure of LA@ZIF-L nanoframeworks induced intracellular ROS

ZIF and its application in the field of biomedicine. This study demonstrated the simultaneous encapsulation of *L. aspera* extract within ZIF-L nanoframeworks and its potential in lung cancer therapy and control of infectious agent. The presence of phytoconstituents of *L. aspera* extract and zinc ions present in ZIF-L exhibits a synergistic effect in ROS induction leading to nuclear damage ultimately causing cancer cell death.

Antibacterial Activity of LA@ZIF-L Nanoframeworks

Antimicrobial efficiency of LA@ZIF-L nanocomposite against the gram positive and negative bacterial strains was evaluated by well-cut method and the results were shown in Fig. 9. Results illustrates that, LA@ZIF-L nanoframeworks exhibited dose dependant increase in antibacterial activity against *B. subtilis, S. aureus, K. pneumonia* and *P. aeruginosa* with highest activity at 100 µg/mL. Comparative analysis of antimicrobial activity of LA@ZIF-L and ZIF-L revealed that LA@ZIF-L exhibited highest growth inhibition against *B. subtilis S. aureus, K. pneumonia and P. aeruginosa* with the zone of inhibition of 18 mm, 20 mm, 17 mm and 21 mm respectively when compared to *L. aspera* extract and ZIF-L alone (Table 1). Antimicrobial activity of LA@ZIF-L nanoframework might be due to synergistic effect of Zn^{2+} ions, imidazole moiety and bioactive compound present in *L. aspera* extract released by enhanced degradation of ZIF-L in nutrient agar and LB medium than water and PBS, caused by interaction of ions and organic constituents in the cell media towards the building block of ZIF-L structure

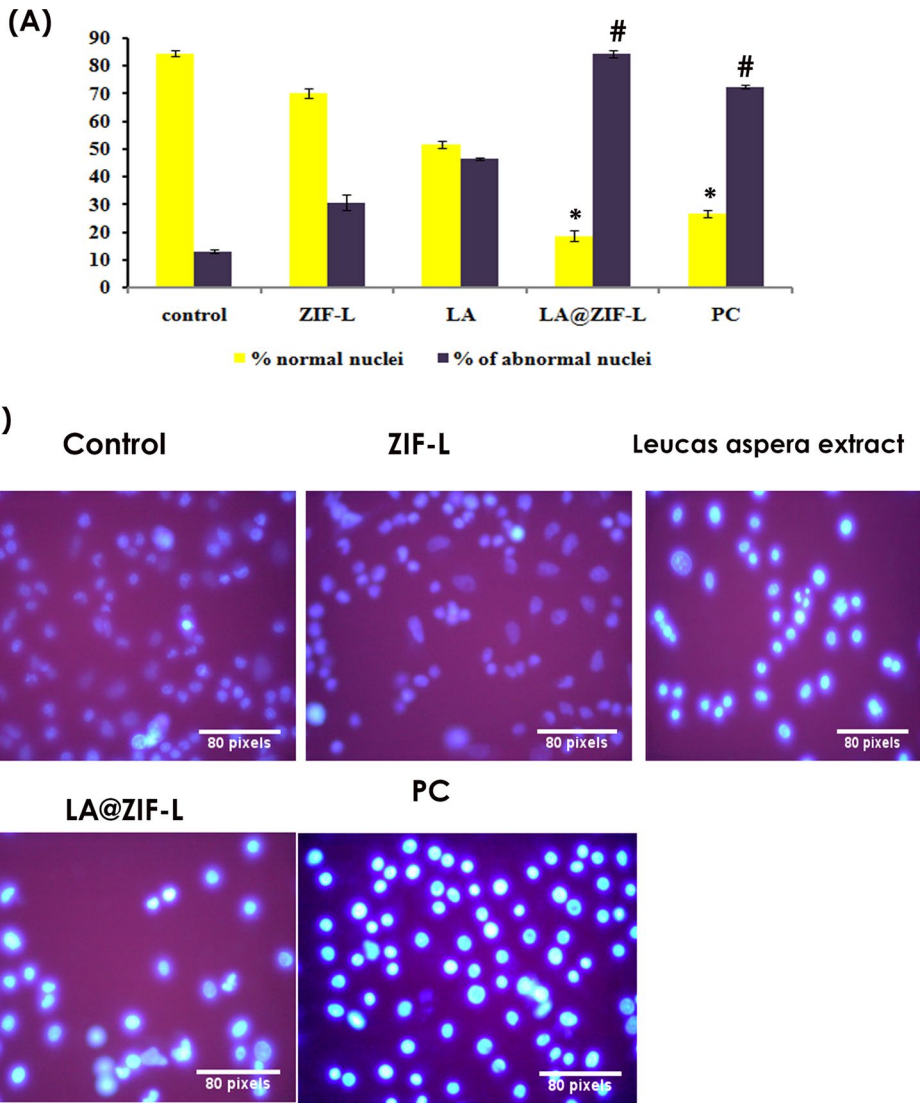

Fig. 8 **A** Quantitative evaluation of normal and abnormal nuclei **B** Microscopic images of nuclear morphology changes of cells treated with LA@ZIF-L nanoframeworks

influencing the hydration-deprotonation equilibrium leading to its quick degradation [41]. Zn^{2+} ions released interact with lipopolysaccharide of bacterial cell wall based on electrostatic force of attraction influencing the fluidity of membrane affecting its integrity facilitating its penetrations inside the bacterial cell. Zn^{2+}ions enhance intracellular ROS leading to apoptosis mediated cell death [42].

MIC value was determined by broth dilution method based on the methodology of Shanholtzer et al., [43]. MIC is the least concentration of LA@ZIF-L which attenuates visible growth of bacteria. Significant ($p < 0.05$) reduction in inoculum viability was observed with increase in concentration of LA@ZIF-L (10 − 2560 µg/mL). MIC for *P. aeruginosa* and *S. aureus* were observed at 320 and 640 µg/mL (Fig. 10A-B).

Bio-Safety Evaluation of LA@ZIF-L Nanoframeworks

Biocompatibility of nanomaterials is major concern for the biomedical applications of nanomaterial as these materials are recognized by the host immune system as non-self agents [44]. Nanomaterials on administration first comes in contact with blood cells, hence Peripheral blood nuclear cells (PBMCs) which constitute 90% of immune cells have been widely used as model system to evaluate the toxicity of nanomaterials [45]. Results of MTT assay revealed that no cytotoxic effects were observed even at the highest dose of LA@ZIF-L NC when compared to vehicle control, while positive control (H_2O_2_100 µM) treated cells exhibited cell viability of 25.5 ± 4.96% (Fig. 11A).

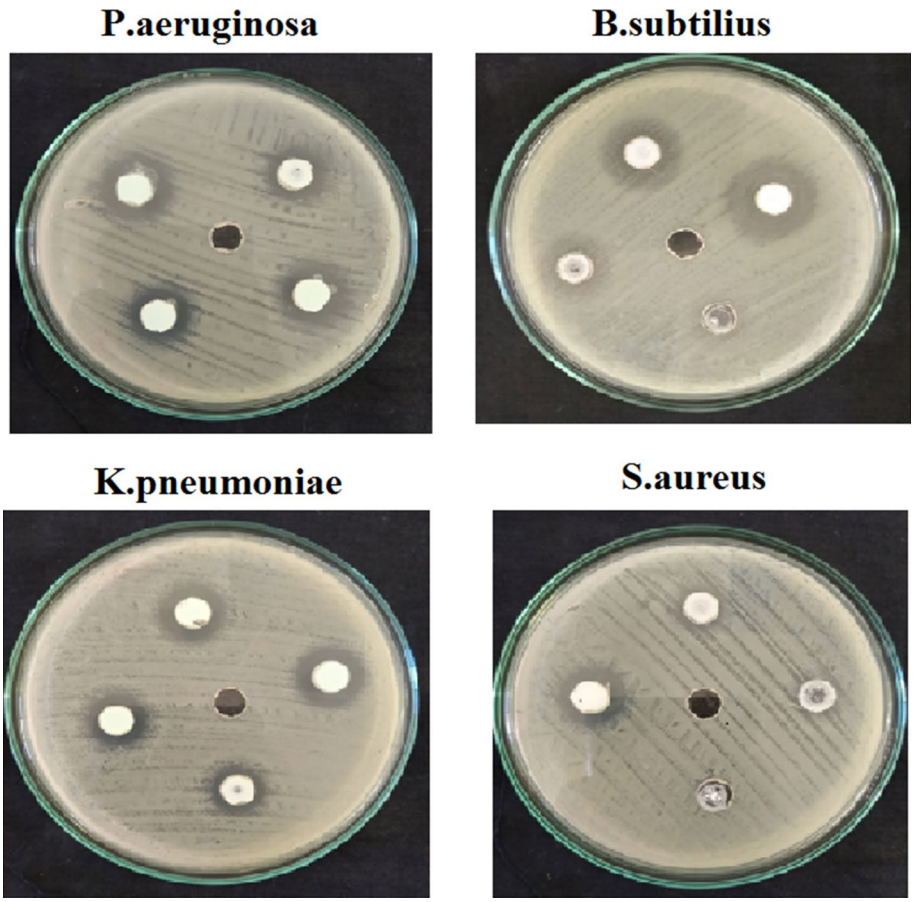

Fig. 9 Comparative analysis of antibacterial potential of LA@ZIF-L nanoframeworks in comparison with bare ZIF-L and *L. aspera* leaf extract

In vivo toxicity studies for LA@ZIF-L nanoframeworks were carried out by using *Artemia salina* as animal model. *A. salina* acute toxicity studies were considered as an alternative low-cost method for acute toxicity studies using animals, which reproduced similar sensitivity as higher animals as per the guidelines of OECD for chemical substances [27, 28]. Results of in vivo toxicity studies of LA@ZIF-L nanoframeworks using *A. salina* were shown in Fig. 11B. Toxicity of a nanomaterial is based on its chemical composition, surface charge and solubility. The results of *A. salina* acute toxicity assay, confirmed that the LC_{50} value of LA@ZIF-L nanoframeworks against *A. salina* nauplii was calculated to be 135.33 ± 2.00 µg/mL. The morphological changes, swimming behavior and malformations of treated groups were examined under the inverted microscope, which showed no significant malformations up to 135 µg/mL. However, at higher doses of 160 and 200 µg/mL, the growth inhibition and with lesser degree of mortality was observed. Overall in vivo toxicity study revealed that LA@ZIF-L nanoframeworks exhibited negligible toxicity at maximum dose of 200 µg/mL. At the end of 48 h post exposure no significant alteration in swimming behavior was observed in all the concentration. In this case, cisplatin-treated groups showed a significant amount of lethality and behavioral changes after treatment. At the highest concentration of cisplatin, 200 µg/mL total damage in internal

Table 1 Antibacterial activity LA@ZIF-L nanoframeworks against clinical pathogens by Well-cut method

Micro organism	Positive control	Zone of inhibition (mm) By the LA@ZIF-L nanoframeworks treated pathogens			*Leucas aspera* leaf extract powder
		25 µg/mL	50 µg/mL	100 µg/mL	
Bacillus subtilis	–	8	12	18	13
Staphylococcus aureus	–	6.3	13.5	20	7
Klebsiella pneumoniae	–	7.5	11.8	17.4	10
Pseudomonas aeruginosa	–	10	13	13.6	9.5

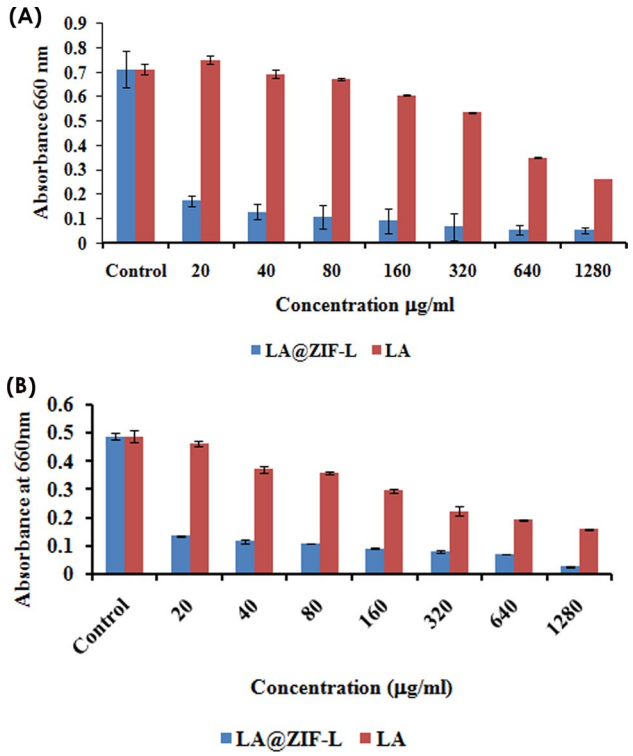

Fig. 10 Minimum Inhibitory Concentration (MIC) of LA@ZIF-L and LA alone against **A** *P. aeruginosa,* **B** *S. aureus*

organs werem observed. Overall, the results of *the Artemia salina* acute toxicity bioassay concluded that LA@ZIF-L nanoframeworks as a biocompatible material suitable for biomedical applications.

Conclusion

The present study revealed that, LA@ZIF-L nanoframeworks synthesized by simple co-precipitation method exhibited significant anticancer and antibacterial efficiency. LA@ZIF-L nanoframeworks exhibited enhanced anticancer and antimicrobial potential due to synergistic effect of LA extract and ZIF-L by enhancing the intracellular ROS level leading to nuclear damage and activation of apoptotic signaling pathway. Results of *A. salina* cytotoxicity study confirmed the biocompatible nature of LA@ZIF-L nanoframeworks. Overall finding of the present investigation highlights that LA@ZIF-L nanoframework as a promising candidate for the treatment of lung cancer and also bacterial borne infectious diseases.

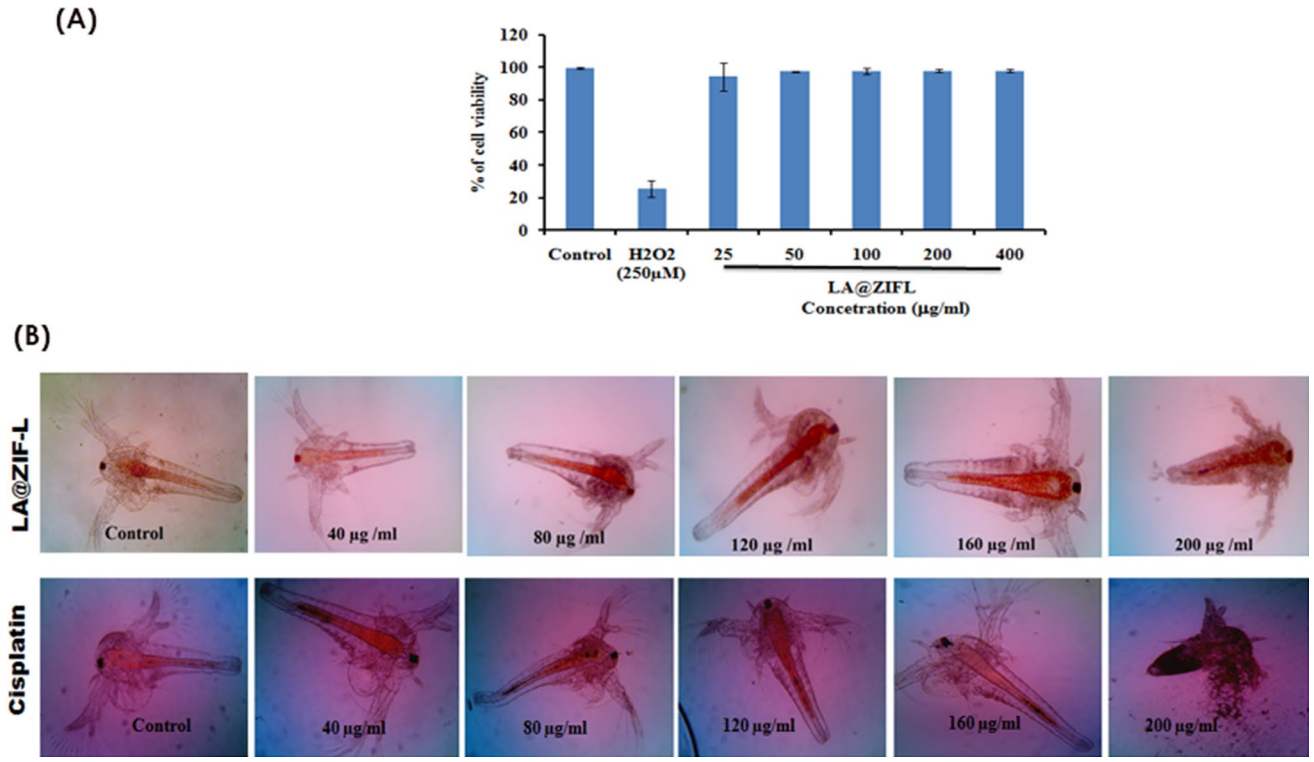

Fig. 11 **A** In vitro cytotoxicity effect of LA@ZIF-L (25—400 µg/mL) in PBMC in comparison with 100 µM H_2O_2 at 24 h; **B** Bio-safety evaluation of *Artemia salina* nauplii post exposure to LA@ZIF-L and positive control Cisplatin at different concentrations (magnification 10x)

Acknowledgements R. Prabhu and N. Suganthy thanks the RUSA-Phase 2.0 grant (No. F. 24-51/2014-U, Policy (TN Multi-Gen), Dept. of Edn. Govt.of India, (Dated: 09.10.2018).

Funding RUSA Phase 2.0, No. F. 24-51/2014-U, Policy (TN Multi-Gen), Dept.

Declarations

Conflict of interest There is no conflict of interest.

References

1. B. P. Biswal, D. B. Shinde, V. K. Pillai, and R. Banerjee (2013). *Nanoscale.* **5** (21), 10556. https://doi.org/10.1039/C3NR03511E.
2. C. Adhikari, A. Das, and A. Chakraborty (2015). *Molecul. Pharmaceutics.* **12** (9), 3158. https://doi.org/10.1021/acs.molpharmaceut.5b00043.
3. C. He, K. Lu, D. Liu, and W. Lin (2014). *J. Americ. Chem. Soci* **136** (14), 5181. https://doi.org/10.1021/ja4098862.
4. J. B. James and Y. Lin (2016). *J. Physic. Chem C* **120** (26), 14015. https://doi.org/10.1021/acs.jpcc.6b01208.
5. C. Y. Sun, C. Qin, X. L. Wang, G. S. Yang, K. Z. Shao, et al. (2012). *Dalton Trans.* **41** (23), 6906. https://doi.org/10.1039/C2DT30357D.
6. A. Tiwari, N. Singh, J. K. Garg, and Randhawa (2017). *Sci. Rep.* **7** (1), 12598. https://doi.org/10.1038/s41598-017-12786-6.
7. C. G. Jones, V. Stavila, M. A. Conroy, P. Feng, B. V. Slaughter, C. E. Ashley, and M. D. Allendorf (2016). *ACS Appl. Mat. Interfac* **8** (12), 7623. https://doi.org/10.1021/acsami.5b11760.
8. W. C. Lee, H. T. Chien, Y. Lo, H. C. Chiu, T. P. Wang, and D. Y. Kang (2015). *ACS Applied. Mate. Interfac* **7** (33), 18353. https://doi.org/10.1021/acsami.5b04217.
9. F. M. Zhang, H. Dong, X. Zhang, X. J. Sun, M. Liu, D. D. Yang, X. Liu, and J. Z. Wei (2017) *ACS Appl Mater Interfaces* **9** (32), 27332. https://doi.org/10.1021/acsami.7b08451.
10. H. Zhang, W. Chen, K. Gong, and J. Chen (2017). *ACS Appl. Mater. Interfaces* **9** (37), 31519. https://doi.org/10.1021/acsami.7b09583.
11. H. Khan (2014). *J. Evid. Based Complement Altern. Med.* **19** (3), 216. https://doi.org/10.1177/2156587214533346.
12. Z. Shinwari (2010). *J. Med. Plant Res.* **4**, 161. https://doi.org/10.5897/JMPR.9000872.
13. A. Datta, C. Patra, H. Bharadwaj, S. Kaur, N. Dimri, and R. Khajuria (2017). *J. Biotech. Biomat.* **7**, 271. https://doi.org/10.4172/2155-952X.1000271.
14. A. Pugazhendhi, R. Prabhu, K. Muruganantham, R. Shanmuganathan, and S. Natarajan (2019). *J. Photochem. Photobiol. B: Biol* **190**, 86. https://doi.org/10.1016/j.jphotobiol.2018.11.014.
15. V. J. Baruah, R. Paul, D. Gogoi, N. Mazumder, S. Chakraborty, et al. (2020). *J Biomolecul Struc Dynamic*. https://doi.org/10.1080/07391102.2020.1844056.
16. A. K. M. Islam and H. Kato-Noguchi (2012). *Inter. J. Sustain Agricul* **4** (1), 01. https://doi.org/10.4236/as.2018.912110.
17. R. Manivannana and D. Sukumar (2007). *Int J Appl Sci Eng* **5**, 133. https://doi.org/10.6703/IJASE.2007.5(2).133.
18. S. Meghashri, H. V. Kumar, and S. Gopal (2010). *Food chem* **122** (1), 105. https://doi.org/10.1016/j.foodchem.2010.02.023.
19. M. S. A. Reza, M. H. Rahman, and T. A. Chowdhury (2020). *Dhaka Univ. J. Sci.* **68** (1), 101. https://doi.org/10.3329/dujs.v68i1.54603.
20. K. Srinivas, M. E. B. Rao, and S. S. Rao (2000). *Indian J. Pharmacol.* **32** (1), 37.
21. Kulandaisamy A. Nirmala and K. Marimuthu (2018). *Syst. Rev. Pharm.* **9** (1), 41.
22. R. Prabhu, R. Mohamed Asik, R. Anjali, G. Archunan, N. M. Prabhu, A. Pugazhendhi, and N. Suganthy (2019). *Process Biochem.* **84**, 39. https://doi.org/10.1016/j.procbio.2019.06.015.
23. R. Prabhu, A. Pugazhendhi, and N. Suganthy (2020). *J Photochem Photobiol B Biol.* **203**, 111774. https://doi.org/10.1016/j.jphotobiol.2019.111774.
24. R. Prabhu and N. Suganthy (2021). *Appl Nanosci*. https://doi.org/10.1007/s13204-021-01881-w.
25. R. Prabhu, B. Karthiyayini, M. Monali, R. Thirumurugan, and N. Suganthy (2022). *J. Drug. Delive. SciTech* **70**, 103223. https://doi.org/10.1016/j.jddst.2022.103223.
26. K. Ilavarasi, P. V. Kiruthiga, S. K. Pandian, and K. P. Devi (2011). *Chemosphere* **84** (7), 888. https://doi.org/10.1016/j.chemosphere.2011.06.017
27. S. Rajabi, A. Ramazani, M. Hamidi, and T. Naji (2015). *Daru* **23** (1), 20. https://doi.org/10.1186/s40199-015-0105-x.
28. S. Rajabi, A. Ramazani, M. Hamidi, and T. Naji (2015). *DARU J. Pharm. Sci.* **23** (1), 20. https://doi.org/10.1186/s40199-015-0105-x.
29. J. Yu and Y. Lu (2018). *Med. Res. Arch.* **6** (2), 1. https://doi.org/10.18103/mra.v6i2.1700.
30. C. J. Wijaya, S. Ismadji, H. W. Aparamarta, and S. Gunawan (2021). *Molecules* **26**, 4416. https://doi.org/10.3390/molecules26154416.
31. P. Foroozandeh and A. A. Aziz (2018). *Nanoscale Res. Lett* **13** (1), 339. https://doi.org/10.1186/s11671-018-2728-6.
32. C. He, Y. Hu, L. Yin, C. Tang, and C. Yin (2010). *Biomaterials* **31** (13), 3657. https://doi.org/10.1016/j.biomaterials.2010.01.065.
33. N. Hoshyar, S. Gray, H. Han, and G. Bao (2016). *Nanomedicine (Lond)* **11** (6), 673. https://doi.org/10.2217/nnm.16.5.
34. A. Saraste and K. Pulkki (2000). *Cardiovasc Res.* **45** (3), 528. https://doi.org/10.1016/s0008-6363(99)00384-3.
35. H. Yang, R. M. Villani, H. Wang, M. J. Simpson, M. S. Roberts, M. Tang, and X. Liang (2018). *J. Exp. Clin. Cancer Res.* **37** (1), 266. https://doi.org/10.1186/s13046-018-0909-x.
36. R. Ishwarya, B. Vaseeharan, S. Subbaiah, A. K. Nazar, M. Govindarajan, et al. (2018). *J. Photochem. Photobiol. B: Biol* **183**, 318. https://doi.org/10.1016/j.jphotobiol.2018.04.049.
37. R. Prabhu and N. Suganthy (2022). *J Inorg Organomet Polym Mat.* https://doi.org/10.1007/s10904-022-02298-w.
38. C. Zhang, X. Wang, J. Du, Z. Gu, and Y. Zhao (2020). *Adv. Sci Weinh.* **8** (3), 2002797. https://doi.org/10.1002/advs.202002797.
39. G. Suganya, S. Karthi, and M. S. Shivakumar (2014). *Parasitol. Res.* **113** (3), 875. https://doi.org/10.1007/s00436-013-3718-3.
40. G. X. Tong, F. F. Du, Y. Liang, Q. Hu, R. N. Wu, J. G. Guan, and X. Hu (2013). *J Mater. Chem. B* **1** (4), 454. https://doi.org/10.1039/C2TB00132B.
41. T. Mahdiar, A. Deepu, S. Tanuka, E. T. Gabriel, V. K. Naresh, A. Tricoli, L. Adrian, R. N. David, and T. Takuya (2020). *Chem. Eng. J.* **413** (1), 12751. https://doi.org/10.1016/j.cej.2020.127511.
42. J. Pasquet, Y. Chevalier, J. Pelletier, E. Couval, D. Bouvier, and M.-A. Bolzinger (2014). *Colloids Surf. A: Physicochem. Eng. Asp* **457**, 263.

43. C. J. Shanholtzer, L. R. Peterson, M. L. Mohn, J. A. Moody, and D. N. Gerding (1984). *Antimicrob. Agents Chemother.* **26** (2), 214.
44. H. Kandárová and S. Letašiová (2011). *Interdiscip. Toxicol.* **4** (3), 107.
45. J. Pourahmad and A. Salimi (2015). *Iran. J. Pharm. Res.* **14** (4), 979.